Long-Term Resilience and Loss Assessment of Highway Bridges under Multiple Independent Natural Hazards

Yaohan Li[1], You Dong[2,*], Dan M. Frangopol[3], and Dipendra Gautam[4]

ABSTRACT

Highway bridges play a significant role in maintaining the safety and functionality of the society. The immediate damage of highway bridges caused by natural hazards can disrupt transportation systems, impede rescue and recovery activities. This disruption may result in tremendous financial and societal losses. Therefore, assessing the vulnerability, recovery capability, potential losses of bridges under natural hazards becomes a primary concern to decision-makers to facilitate the emergency response and recovery efforts. Under these concerns, resilience is a paramount performance indicator to evaluate and recover the functionality of structural systems under extreme events. In this paper, an integrated framework for long-term resilience and loss assessment of highway bridges under multiple independent natural hazards is presented. The impacts of extreme events such as earthquakes, hurricanes and floods on the life-cycle performance of bridges are illustrated. A stochastic renewal process model of the random occurrence of hazard events is used to compute the expected long-term resilience and damage loss by considering both time-independent and time varying occurrence characteristics. The proposed approach is applied to a highway bridge, in which the impacts of earthquake and hurricane hazards are considered. This framework can be implemented to the design, maintenance, and retrofit optimization of infrastructure systems under multiple extreme events.

Keywords: Resilience; Long-term loss assessment; Highway bridges; Multiple natural hazards

[1] Research Assistant and Ph.D. student, The Hong Kong Polytechnic University, Department of Civil and Environmental Engineering, Hung Hom, Kowloon, Hong Kong, yaohan.li@connect.polyu.hk.
[2] Assistant Professor of Structural Engineering, The Hong Kong Polytechnic University, Department of Civil and Environmental Engineering, Hung Hom, Kowloon, Hong Kong, you.dong@polyu.edu.hk. *Corresponding Author.
[3] Professor and the Fazlur R. Khan Endowed Chair of Structural Engineering and Architecture, Department of Civil and Environmental Engineering, Engineering Research Center for Advanced Technology for Large Structural Systems (ATLSS Center), Lehigh University, 117 ATLSS Dr., Bethlehem, PA 18015-4729, USA, dan.frangopol@lehigh.edu.
[4] Structural and Geotechnical Dynamics Laboratory, StreGa, DiBT, University of Molise, Campobasso, Italy, email: dipendra.gautam.seri@gmail.com.

1 Introduction

Highway bridges are essential infrastructure components to ensure safety and functionality of the society. During their service life, bridges are exposed to multiple hazards such as earthquakes, floods, and hurricanes. The resulting structural damage can cause significant disruption to transportation systems and substantial economic loss to the society. In a long-term perspective, it is likely that the potential risk and loss are accumulated and aggravated due to uncertainties throughout the entire life-cycle of civil infrastructure systems. Therefore, risk mitigation for highway bridges has received an increasing awareness from researchers, policy-makers, and insurers in terms of the importance of assessing the performance, recovery capability and long-term loss of bridges under natural hazards. Though the reliability of infrastructure systems with respect to external disasters has been emphasized in previous studies (Akiyama *et al*. 2011; Thanapol *et al*. 2016), the ability of bridges recovering functionality to acceptable levels under multiple extreme events has not been explored extensively and more studies are required on resilience quantification. Therefore, it is necessary to provide a comprehensive resilience and probabilistic loss assessment of highway bridges under natural hazards to aid the preparation of emergency response and recovery decisions.

To mitigate the impacts of extreme hazards, structural resilience is expected to be enhanced towards a desired level by considering structural functionality before, during, and after an extreme event. Resilience, related to the functionality of structural systems under extreme events and recovery patterns, is becoming a paramount performance indicator within the hazard management process (Bruneau *et al.* 2003; Bocchini and Frangopol 2011; Frangopol 2011; Frangopol and Soliman 2016; Frangopol *et al.* 2017; Zheng and Dong 2019). It highlights the evaluation of capability of civil infrastructure systems to maintain prescribed safety, flexibility, and to recover from extreme events. Several definitions of resilience were proposed in the literature. One of the most widely used definitions was provided by Bruneau *et al.* (2003): “Resilience is defined as the ability of social units (e.g., organizations, communities) to mitigate hazards, contain the effects of disasters when they occur, and carry out recovery activities in ways that minimize social disruption and mitigate the effects of future earthquakes”. Resilience has four properties: robustness, rapidity, redundancy, and resourcefulness. Robustness is the strength or the ability of units to withstand a certain level of stress without suffering degradation or loss of function; Redundancy is the ability

of satisfying functional requirements when disruption, degradation, or loss of functionality occurs; Resourcefulness is the ability to apply material and human resources to achieve established priorities, resources mobilization and other goals; Rapidity is the capacity to achieve priorities and other goals in a timely manner to reduce the losses and avoid future disruption (Bruneau *et al.* 2003).

The previous studies on resilience were mainly focused on the assessment of bridges associated with single-hazard analysis. Decò *et al.* (2013) and Dong and Frangopol (2015) assessed the resilience of highway bridges under seismic hazard. The resilience of bridges under flood effects with different return periods was investigated by Dong and Frangopol (2016). There were a limited number of resilience studies of bridges dealing with multiple hazard effects (Decò and Frangopol 2011; Pescaroli *et al*. 2018; Akiyama *et al.* 2019). Multiple hazards could bring considerably more disastrous consequences to the society than a single hazard (Padgett *et al.* 2009; Jalayer *et al.* 2011; Dong and Frangopol 2017; Zheng *et al.* 2018). Gidaris *et al*. (2017) underlined that structural vulnerability, loss evaluation, recovery and restoration models were key elements for accurate quantification of resilience of highway bridges in the multihazard analysis. Bruneau *et al*. (2017) reviewed the state of the art of structural performance under multiple hazards by considering the resilience and hazard interaction effects were highlighted for different structural systems. This work indicated that further efforts should be implemented to explore the multihazard performance in a life-cycle context for a variety of hazards and structural portfolios. In the long-term performance evaluation of highway bridges, uncertainties associated with vulnerability, loss and resilience can be accumulated due to different occurrence probability of different hazardous events. Under the multihazard consideration, different indicators may show various performance characteristics of a range of hazardous events. Thus, it is essential to incorporate consideration of multiple hazards into performance studies of structures and civil infrastructure systems to identify the most dominant and costliest hazard scenario to help decision-makers propose the optimal design and management strategies.

Most of previous studies on the resilience assessment focused on some given hazard scenarios without considering the stochastic process of the hazard occurrence within the service life of structures except for a few (Yang and Frangopol 2019a). In this paper, the probabilistic long-term resilience and loss considering time-dependent interarrival time models are assessed. Though the concept of long-term resilience was introduced by Yang and Frangopol (2019a), specific physical-

informed damage models were not taken into account. Pandey and Van der Weide (2017) introduced the general renewal process to formulate the lifetime damage cost of a structure. This cost was considered as the only performance indicator in the renewal process without considering the long-term resilience. Generally, both the resilience and loss are important indicators for decision-makers to propose the optimal management strategies under multi-hazard considerations. Although the approach proposed by Pandey and Van der Weide (2017) considered time-dependent interarrival models, the analytical model was not validated by the numerical simulation. To address these concerns, this paper aims to present a comprehensive framework to quantify the long-term resilience and loss of highway bridges under different natural hazards, incorporating both time-independent and time-varying interarrival models of hazard occurrence using renewal process. Monte Carlo simulations are conducted to validate results from the proposed renewal-based approach.

Overall, in this paper, an integrated framework quantifying long-term resilience and loss of highway bridges under natural hazards is presented. Independent natural hazards are focused. The proposed framework presents the process of considering multiple hazard impacts into the resilience and loss assessment, including the stochastic process of hazard occurrence, structural vulnerability analysis, functionality analysis and life-cycle analysis. Insights and lessons learnt from past extreme events are outlined to emphasize the significance of resilience and loss assessment under hazards. Damage assessment of highway bridges associated natural hazards including earthquakes, hurricanes and floods and structural performance is introduced. An illustrative example is provided to introduce the evaluation of long-term resilience and loss of a typical highway bridge under representative hazard scenarios of earthquakes and hurricanes. A numerical model of the highway bridge is established to evaluate the structural performance under hurricane hazard. An experimental study is conducted to validate the numerical bridge model.

2 **Resilience Assessment**

Catastrophic damages caused by recent natural hazards such as Hurricane Katrina and Hurricane Michael and other natural disasters worldwide raised awareness of the public to the importance of risk mitigation and resilience assessment on transportation systems (Zhang *et al*. 2017; Zhang *et al*. 2018; Kilanitis and Sextos 2019; Yang and Frangopol 2019b). Resilience, as an important

structural performance indicator, is defined as the ability of a civil infrastructure system to maintain its functionality and return to normality after an extreme event. A resilience assessment establishes a connection between structural performance, post-hazard functionality, and recovery. Typically, this assessment comprises identification of multi-hazard risks, resilience analysis, and evaluation of resilience as shown in Figure 1 (ISO 2009).

Risk assessment plays an important role as risk is related to both the consequences caused by structural failure or loss of functionality associated and probability of structural failure. The outputs of communication are used to assess the risk and resilience effectively by establishing the context. Subsequently, cumulative risk and resilience of the given infrastructure system could be obtained under multiple natural hazards. Once resilience assessment is conducted, evaluation in terms of resilience parameters and their acceptability and viability should be performed. It is worth noting that performance parameters and countermeasures may vary in time and space at local scale due to the interaction between resilience and risk. The proposed framework allows decision-makers and practitioners to assess and enhance the resilience of structures and to propose rational actions associated with planning, maintenance and rehabilitation against natural hazards. These actions generally consist of social measures (e.g., awareness), physical measures (e.g., infrastructural preparedness) and corrective measures (e.g., life-cycle assessment of retrofitting decisions). In addition to analysis, continuous monitoring and periodic review are essential. An adaptable process of resilience assessment is required to encapsulate changes in contexts and record continuous evolution of resilience, as indicted in Figure 1.

Resilience has been increasingly implemented to performance-based seismic design of bridges as a vital performance indicator (Frangopol *et al.* 2017; Zheng and Dong 2018; Broccardo *et al.* 2015). Embedding resilience within performance-based design could incorporate more decision variables (e.g., repair cost, time) within structural design process. For example, additional factors can be included in the design procedures such as social and financial implications, recovery from a damage state or collapse, among others.

A probabilistic model that can be used in the performance-based bridge design under multiple hazards is (Moehle and Deierlein 2004)

$$\begin{aligned} &\mathrm{P}(D > dv \mid IM = im) \\ &= \int_{dm}\int_{edp}\int_{im} G_{DV|DM}(dv \mid dm).|\, dG_{DM|EDP}(dm \mid edp).|\, dG_{EDP|IM}(edp \mid im)|.|\, dG_{IM}(im)| \end{aligned} \quad (1)$$

where P indicates the aggregate probability of a structure reaching or exceeding the limit state; *DM* indicates the damage measure; *EDP* indicates the engineering demand parameter; *IM* indicates the intensity measure; and *DV* indicates the decision variables. The Eq. (1) is a significant part of the PEER framework (PEER 2013) from the Pacific Earthquake Engineering Research Center (PEER). Broccardo *et al*. (2015) validated the effectiveness of using the PEER framework to assess the probabilistic resilience of civil systems. Incorporating the resilience as a decision variable, the PEER framework satisfied the optimal target under the investigated hazard through accomplishing of resilience management strategies. Additionally, different decision variables can be implemented based on this framework. A recent case study of reinforced concrete buildings presented a systematic analysis integrating resilience, sustainability and loss into the PEER framework (Hashemi *et al*. 2019). Apart from seismic hazard, the integrated framework has been applied to other different hazard types, such as coastal bridges against extreme wave-induced loads. Qeshta *et al*. (2019) provided a review of resilience assessment on coastal bridges against extreme wave-induced loading, in which studies were comprehensively concluded in terms of wave forces, bridge response, vulnerability analysis, and resilience assessment incorporating with the PEER framework. Different from earthquakes, the hurricane-induced impact upon bridges is a typical example of concurrent multi-hazard event, as bridges are affected by wind, storm surge, and waves simultaneously. Therefore, instead of focusing on the single intensity measure, (e.g., peak ground acceleration of seismic hazard), the integrated assessment framework under hurricanes requires multiple independent or correlated intensity measures, such as wave height, wave period, clearance, and inundation depth. Zhang and Alam (2019) indicated that damage to bridges can be additionally considered at transportation levels besides the commonly defined structural levels. The structural level damage comprises the losses arising from bridge repair. Similarly, transportation level damage accounts for the serviceability of bridges leading to indirect loss such as traffic delays and detour (Yang and Frangopol 2018). Meanwhile, due to continuous exposure to the traffic, it is likely that the indirect loss caused by transportation damage would fairly surpass the direct loss resulted from structural damage. These examples have provided effective approaches for the multi-hazard considerations. Overall, various metrics can be selected into the performance-based studies

of structures and civil infrastructure systems in the multi-hazard analysis. The resilience model provided by Bruneau *et al*. (2003) gives

$$R_{Resi} = \frac{1}{\Delta t_r} \int_{t_0}^{t_0+\Delta t_r} Q(t)dt \tag{2}$$

where $Q(t)$ is the functionality of a bridge under recovery function at time t (e.g., days); t_0 is the initial investigated time; and Δt_r is the investigated time interval. The functionality is significant during the resilience quantification as restoration of structure highly depends on how the repair and recovery work. Functionality levels can be defined to classify the emergency response and recovery post-earthquake period. For example, for the planning of emergency response, the functionality can be considered as the capability of a bridge located on a link transferring resources to hazard affected areas. With respect to the recovery at post-earthquake phase, the functionality can be considered in different stages as open, limited use, and closed. The expected functionality is evaluated from that associated with the investigated damage states. There are several models available for the functionality quantification. Decò *et al*. (2013) proposed an effective probabilistic model to compute the time-dependent functionality of bridge after a seismic event based on six probabilistic parameters including uncertainties. However, implementation of this comprehensive approach can be challenging when there is limited information available. Cimellaro *et al*. (2010) indicated that the functionality computational process could be classified based on the community preparation levels, while quantification of these levels might be difficult during the multiple-hazard analysis. These community preparation levels were classified as prepared community, not well-prepared community, and well-prepared community, respectively. Another efficient recovery model was proposed by ATC (1999) to assess the functionality restoration process of bridges based on lognormal cumulative distributed function (CDF). This method allows quantification of functionality under the given recovery pattern and requests the least inputs compared to the other approaches.

The recovery models for earthquakes are widely investigated, whereas there is limited research on the recovery models of coastal bridges under hurricanes. The majority of recovery models applied to the hurricane-induced damages are based on the seismic restoration methodologies and tsunami-based approaches (Gidaris *et al*. 2017). For instance, Bocchini and

Frangopol (2012) proposed the functionality recovery model considering various restoration scenarios using a sinusoidal process. Though different performance stages are evaluated, it is difficult to calibrate the parameters used in this recovery model, as there is large uncertainty in the damage collection. When considering the hurricane-induced waves and surge, a HAZUS tsunami approach (FEMA 2013) can be utilized, which presents a framework based on expert opinion survey to evaluate the loss being in different damage states. However, the HAZUS approach is a simplified model as the bridge is assumed to be restored to full performance rather than different levels. Qeshta *et al*. (2019) indicated that some seismic restoration models can be applied to the other types of natural hazard (e.g., damaged bridges by hurricanes).

Another resilience model introduced by Minaie and Moon (2017) focused on the practical implementation of resilience assessment and proposed a simplified resilience quantification framework of bridges under extreme events. The bridge resilience is illustrated as the capability of a bridge to maintain a robustness level and to recover to a target performance level within the shortest time. Robustness refers to the residual performance subsequent to a natural hazard, which can be computed by integrating hazard, vulnerability, and uncertainties (Minaie and Moon 2017)

$$P_R = 100\% - \max(9.259 \times H \times V \times UF) \times I \tag{3}$$

in which I represents importance factor of the investigated bridge; H is related to the hazard severity; V refers to the vulnerability, the product $H \times V$ depends on each extreme event and vulnerability category; and UF is the uncertainty factor. Through this equation, the robustness could represent the worst potential scenario affecting bridge functionality. A simplified model of recovery is provided considering the recovery time as a function of adjustment factors and restoration, in which the recovery time is adjusted based on the management practices from agency, historical records of extreme events in the past year, and bridge types. Accordingly, for a control time within one year (i.e., 365 days), the bridge resilience can be evaluated as the ratio of the area of the post-event performance to the area under the desired performance level (e.g., 100% for full recovery)

$$R = \frac{\int_{t_0}^{t_0+365days} P(t)dt}{\int_{t_0}^{t_0+365days} P(100\%)dt} \quad (4)$$

where $P(t)$ refers to the structural performance and $P(100\%)$ is the optimized performance. This engineering-based resilience quantification method efficiently assesses the resilience capturing key parts of bridge operation, knowledge of experts, and lessons learnt from past disruptive events. In addition to the two methods presented in Eqs. (2) and (4), there are several other effective models available for the resilience assessment in the literature (e.g., Franchin and Cavalieri 2015).

3 Resilience and Structural Damage Loss Estimation under Hazards on a Long-Term Vision

This section aims to provide a long-term assessment framework of highway bridges with respect to resilience and structural damage loss under natural hazards. During the life-cycle analysis, the large uncertainty related to the frequency and intensity of natural hazards in the life-cycle analysis can be quantified by the stochastic occurrence model. In literature, although the homogeneous Poisson process (HPP) has been widely used to model hazard occurrence, the stochastic characteristics of natural hazards are limited to time-independent property. To incorporate both time-independent and time-varying occurrence characteristics, this paper adopts a renewal process (a generalization of HPP) to assess the long-term resilience and loss.

Given the investigated time period $(0, t_{\max}]$, each hazard event (e.g., earthquake) occurring within this period is described using index k. T_k denotes the arrival time of hazard, L_k is the economic loss, and R_k refers to the bridge resilience under investigated hazard. Interarrival time is defined by W_k, where arrival time equals the sum of interarrival times $T_k = W_1 + W_2 + \ldots + W_k$. The hazard occurrence is modeled by the renewal process, where the interarrival time W_k is independently identically distributed (IID). The time period $t_{\max}$ can be taken as the lifespan of infrastructure and the total number of hazard occurrence is $N(t_{\max})$, with $T_k \leq t_{\max}$. An illustrative diagram illustrating the long-term resilience and loss framework is shown in Figure 2. Based on the established stochastic model, the long-term resilience $\mathrm{RE}_{lt}(t_{\max})$ within investigated period $t_{\max}$ can be written as

$$RE_{lt}(t_{\max}) = \sum_{k=1}^{N(t_{\max})} R_k \tag{5}$$

in which R_k is the bridge resilience associated with a single hazard and $N(t_{\max})$ is the total number of hazard occurrences within investigated service life. The long-term resilience is the sum of resilience of all the hazard events. In addition to the resilience, the long-term loss can also be evaluated based on the renewal process. The cumulative long-term damage loss $DL_{lt}(t_{\max})$ can be formulated as

$$DL_{lt}(t_{\max}) = \sum_{k=1}^{N(t_{\max})} L_k e^{-rT_k} \tag{6}$$

where L_k is the economic repair loss; T_k is the arrival time of the *kth* hazard; and the financial discount rate r is used to transform future damage loss into the present within the investigated time horizon. Long-term loss is discounted to the present value using a constant discount rate r.

The long-term resilience and loss can be quantified by using analytical computation and numerical Monte Carlo (MC) simulations, but the simulation approach can be expensive. Analytically, the expected long-term resilience and loss can be quantified analytically using the properties of renewal theory (Ross 2014). The key to solve Eqs. (5) and (6) is to identity the number of hazard events, which can be expressed as

$$E[N(t_{\max})] = \sum_{k=1}^{\infty} F_W^{(k)}(t_{\max}) = \Phi(t_{\max}) \tag{7}$$

in which $F_W^{(k)}(t_{\max})$ is a k-fold convolution of interarrival time W_k and $\Phi(.)$ is known as the renewal function in the renewal process.

The renewal function satisfies an integral equation conditioning on the first arrival time y. The CDF of interarrival time $F_W(t)$ is assumed to be continuous. Hence, the expected number of events denoted by a density function yielding at the first renewal $dF_W(y)$ can be written as

$$\Phi(t_{\max}) = E[N(t_{\max})] = \int_0^{\infty} E[N(t_{\max}) \mid W_1 = y] dF_W(y) \tag{8}$$

When the first arrival time is larger than $t_{\max}$, there is no event within the investigated period, with $E[N(t_{\max})] = 0$. When $y \leq t_{\max}$, the renewal process enables the renewals have the same distribution. Hence,

$$E[N(t_{\max}) \mid W_1 = y \leq t_{\max}] = 1 + E[N(t_{\max} - y)] = 1 + \Phi(t_{\max} - y) \tag{9}$$

Substituting Eq. (9) into the Eq. (8), the expected number of arrivals can be written as

$$\Phi(t_{\max}) = F_W(t_{\max}) + \int_0^{t_{\max}} \Phi(t_{\max} - y) dF_W(y) \tag{10}$$

Using the renewal function, the expected long-term resilience and loss can be formulated as follows

$$E[RE_{lt}(t_{\max})] = E[R]\Phi(t_{\max}) \tag{11}$$

$$E[DL_{lt}(t_{\max})] = E[L]\int_0^{t_{\max}} e^{-rt} d\Phi(t) \tag{12}$$

in which $E[N(t_{\max})]$ is the expectation of the number of hazard events within bridge service life. The derivations of Eqs. (11) and (12) are shown in Appendix A. It is assumed that damaged bridge is repaired to the pre-damage state before the next hazard event.

Given $E[N(t_{\max})] = \lambda t_{\max}$ based on the Poisson-based renewal process, the expected long-term resilience and loss associated with Poisson process can be formulated as

$$E[RE_{lt}(t_{\max})] = R\lambda t_{\max} \tag{13}$$

$$E[DL_{lt}(t_{\max})] = \frac{L\lambda}{r}(1 - e^{-rt_{\max}}) \tag{14}$$

in which the expected resilience of each hazard event and economic repair loss are defined as $E[R] = R$ and $E[L] = L$.

In earthquake engineering, there are several other nonstationary renewal processes adopted with time-varying interarrival time models except exponential models. For instance, a Brownian model is increasingly used in the long-term seismic analysis and forecasting (Matthews *et al*. 2002). The interarrival time follows Brownian passage-time (BPT) distribution with a probability density function (PDF)

$$f_W(t) = \left(\frac{\mu}{2\pi\alpha^2 t^3} \right)^{1/2} \exp\left\{ -\frac{(t-\mu)^2}{2\mu\alpha^2 t} \right\} \tag{15}$$

where μ is the mean and α is coefficient of variation (COV). The long-term resilience and loss based on the renewal BPT model can be computed using Eqs. (10) to (12), where the expected number of hazards are computed by the integration. The CDF of BPT distribution is provided in Matthews *et al*. (2002). Based on the proposed renewal approach, a variety of time-varying interarrival time models can be applied into the assessment of long-term resilience and loss, such as Gamma (Hainzl *et al*. 2006) and lognormal (Michael 2005) distributions.

4 **Evaluating Natural Hazards for Bridges**

The multi-hazard consideration in risk analysis has been gaining momentum since early 2010 due to increasing exposure of highway bridges to multiple hazards. Studies of Decò and Frangopol (2011), Kameshwar and Padgett (2014), Wang *et al*.(2014), Liao *et al*. (2018), Akiyama *et al*. (2019) incorporated the effects of multiple natural hazards on highway bridges. When considering the interactive impacts of these extreme events, one key aspect of multi-hazard analysis is to involve both independent (e.g., an earthquake and environmental-induced corrosion) and interacting (e.g., an earthquake triggering the subsequent tsunami) hazard scenarios into the assessment (Akiyama *et al*. 2019; Gautam and Dong 2018). In order to assess the structural performance under multiple hazards, an integrated consideration is necessary consisting of the probability of hazard occurrence, vulnerability of the structural system under hazards, and consequences of structural failure, as indicated in Figure 3. In this study, the independent natural hazards are considered. Given more information regarding the interacting effects associated with multiple hazards (e.g., occurrence probability, vulnerability analysis under multiple hazards), the

dependent hazards could also be assessed. A detailed illustration regarding damages of highway bridges associated with earthquake, hurricane and floods hazards is provided in this section.

4.1 *Earthquakes*

Earthquake is a typical hazard for structural systems. In the probabilistic seismic hazard analysis (PSHA), seismic intensity at the location of structure should be identified at the beginning. The analysis procedure associated with PSHA using the ground motion prediction equation is demonstrated in Appendix B. The seismic vulnerability of structural systems could be computed based on structural analysis. The vulnerability of a structural system could be addressed through fragility curves that indicate the probability of reaching or exceeding a particular damage state under the designated intensity measure (*IM*) level.

The fragility curves can be calculated as (Cornell 2002)

$$\mathrm{P}[DI \geq LS_i \mid IM] = 1 - \int_0^{LS_i} \frac{1}{\sqrt{2\pi} \cdot \xi_{EDP|IM} \cdot edp} \cdot \exp\left(-\frac{[\ln(edp) - \ln(a \cdot IM^b)]^2}{2(\xi_{EDP|IM})^2}\right) d(edp) \qquad (16)$$

where LS_i represents the ith LS and $\xi_{EDP|IM}$ is the standard deviation of the logarithmic distribution. The seismic demand assesses the *EDP* as a function of a chosen ground motion intensity and can be quantified using appropriate seismic structural responses, such as deformation or ductility of vulnerable components. For highway bridges, reinforced concrete (RC) columns are key components susceptible to seismic damage. Sectional curvature ductility, displacement ductility, and residual displacement are commonly used as the seismic damage indicators for RC columns.

4.2 *Hurricanes*

The impact of hurricanes upon highway bridges shows a typical example of interacting multi-hazard effects. For instance, the bridge is threatened by concurrent hazards during a hurricane event including strong wind, wave and storm surge. In this section, two methods of evaluating hurricane-induced damage are introduced consisting of analytical and numerical studies.

The effects of hurricanes on highway bridges mainly stem from storm surge and wave-induced loading. The resulting uplift forces in vertical and horizontal directions produce large displacements at supports. When the displacements surpass the limitation at supports, the deck

unseating may occur (Mondoro *et al*. 2017). It is commonly recognized that deck unseating failure is the most primary damage for simply and continuous supported bridges (Kulicki 2010). Some bridge spans even with fixed connection using dowelling undergo complete connectivity failure during the Hurricanes Katrina (Padgett *et al*. 2008). Wang *et al.* (2017) recommended a method to assess hurricane-induced structural damage loss from the perspective of insurers and performed a hurricane vulnerability analysis considering model uncertainty. This paper presents a probabilistic life-cycle assessment framework of bridges vulnerable to hurricanes and suggests a new approach for damage loss assessment under hazards. The hurricane can be considered through the probability distribution of the wind speed *V*. The associated CDF with time-variant parameters $u(t)$ and $\alpha(t)$ is (Wang *et al.* 2017)

$$F_v(v,t) = \Pr(V < v) = 1 - \exp\left[-\left(\frac{v}{u(t)}\right)^{\alpha(t)}\right] \tag{17}$$

The vulnerability analysis indicates estimation of the probability of failure of bridges under the given hurricane scenarios. In structural safety analysis, failure occurs when the demand surpasses capacity. This paper highlights the deck unseating failure mode for bridges during hurricanes. Deck unseating occurs when the capacity of bridge superstructure at supports fails to resist the uplift forces caused by storm wave loadings. These variables can be obtained from either empirical methods or computational modelling. Both methods can provide relatively accurate approximations of wave forces upon bridge deck. The empirical method provides the maximum wave force through time-independent computation, while the computational approach can provide the time-variant wave forces. However, the latter approach is usually computationally expensive.

The American Association of State Highway and Transportation Officials (AASHTO) provided guide specifications for bridges vulnerable to coastal hurricanes (AASHTO 2008; Mondoro *et al*. 2017). In these specifications, a set of equations assessing maximum vertical force, maximum horizontal force and the corresponding overturning moment, are formulated. The vertical loading on bridge superstructure contributes to deck unseating failure. According to AASHTO (2008), the maximum quasi-static vertical force is defined as

$$F_{v-\max} = \gamma_w \bar{W} \beta (-1.3 \frac{H_{\max}}{d_s} + 1.8)[1.35 + 0.35 \tanh(1.2(T_p) - 8.5)]$$
$$(b_0 + b_1 x + \frac{b_2}{y} + b_3 x^2 + \frac{b_4}{y^2} + \frac{b_5 x}{y} + b_6 x^3)(TAF) \quad (18)$$

where γ_w represents the unit weight of water; $H_{\max}$ refers to the maximum wave height; d_s is the water depth at or near the bridge; T_p is the wave period; W is the defined wetted deck width; β is a coefficient associated with the wave crest and bridge deck; x and y are defined as the ratio of maximum wave height over wave length and the ratio of deck width over wave length, respectively; b_0 to b_6 are coefficients associated with bridge deck spans; and TAF is the trapped air factor considering the effect of trapped air. The significant wave height and wave period are required to compute the demand of bridge deck. The vulnerability model associated with hurricane wind speed aims to characterize the probability of bridge deck unseating damage caused by hurricanes. Subsequently, Monte Carlo simulation and/or other computational analysis methods can be applied to attain the probability of failure.

In addition to the empirical model, the computational approach, referring to the computational fluid dynamics (CFD) model, could also be used to compute the forces on the superstructure. It provides simulations of 2D/3D hydrodynamic modelling. During the dynamic fluid interactions, the movement of fluid in physical domain depends on various properties. Changes of these characteristics are commonly examined by the Navier-Stokes equations based on laws of conservation (Temam 1984). In terms of the structural simulation, the total force along a designated force vector equals to the sum of dot product of the viscous forces and pressure horizontally and vertically. This relationship is (Kohnke 1994)

$$F_a = \vec{a} \cdot \overrightarrow{F_p} + \vec{a} \cdot \overrightarrow{F_v} \quad (19)$$

where $\vec{a}$ is the designated force vector; $\overrightarrow{F_p}$ is the pressure force vector; and $\overrightarrow{F_v}$ is the viscous force vector.

4.3 *Floods*

Highway bridges are particularly susceptible to floods especially in coastal areas. Several historical events have highlighted that floods can be disastrous to bridge structures (Gautam and Dong 2018).

For instance, the 2017 central Nepal flash flood washed away a bridge (see Figure 4a) due to torrential precipitation of four hours. Although the bridge was built recently (completed in June 2015), the debris with the flash flood in the mountainous terrain was particularly destructive and the bridge disappeared without any signature on site. According to the records of flooding events, it is found that bridges are extensively damaged due to flash floods. Forensically, it could be inferred that the damage due to flash floods would surpass the damage due to earthquakes having moderate ground shaking. Flood impact to bridges can be attributed to scour, deterioration of bridge components, water pressure, hydrodynamic forces exposed to the bridge/component, and debris impact and accumulation, among others. Bridge scour, deterioration, and increment of water pressure due to debris accumulation are considered as the major detrimental factors. Increased hydrodynamic forces together with debris and sediments usually cause bridge scouring (see Figure 4b), particularly in piers.

Deterioration due to various factors is another notable problem that causes functionality loss or collapse of bridges. In general, environmental conditions, lack of drainage, load fluctuation above the capacity, and lack of periodic maintenance can cause deterioration of bridge components. Occasionally, significant deterioration may lead to serious compromise in the functionality as well. Bridges built in developing countries are more likely to suffer from deterioration aggravation compared to those in developed areas due to lack of preventive maintenance as well as emergency maintenance strategies. Additionally, deteriorated bridges are more vulnerable than the non-deteriorated counterparts. For instance, the 1988 and 2015 earthquakes in Nepal highlighted that similar type of bridges close to the epicenter performed better during the 1988 earthquake than the bridges far from the epicenter during the 2015 Gorkha, Nepal earthquake. Compared to the deficient behavior during the 2015 earthquakes, the performance of bridges was satisfactory during the 1988 earthquake. This is most likely attributed to the age of bridges. Aging can lead to decrease of structural capacity and increase in bridge vulnerability (Gautam 2017).

Corrosion of reinforcement usually occurs due to environmental conditions. Thoft-Christensen *et al*. (1997) suggested the reduction in reinforcement area considering a time-dependent model as

$$A(t)=\begin{cases}\dfrac{\pi D^2}{4} & \text{for } t \le T \\ \dfrac{\pi D(t)^2}{4} & \text{for } T < t < T+\dfrac{D}{r_1} \\ 0 & \text{for } t \ge T+\dfrac{D}{r_1}\end{cases} \tag{20}$$

In Eq. (20), $A(t)$ indicates the effective area of the reinforcement; D is the diameter of reinforcement; T is the time when corrosion starts; r_1 is the rate of corrosion; and $D(t)$ is the effective reinforcement diameter after t years. Furthermore, $D(t)$ can be calculated using Eq. (21) as follows

$$D(t)=D-r_1\times(t-T) \tag{21}$$

Due to high velocity of water together with the debris and sediments, increased water pressure also becomes prevalent to bridges. AASHTO (2000) suggested estimation of water pressure based on the empirical formula

$$p_w=5.14\times10^{-4}\times C_D\times v^2 \tag{22}$$

where p_w is the water pressure and C_D is the drag coefficient. The scour depth for a single pier can be estimated using the empirical formula suggested by (Yanmaz 2001)

$$S=1.564\times\chi^{0.405}\times\left(\frac{v}{\sqrt{g\times d}}\right)^{0.413} \tag{23}$$

where S is the scour depth; χ refers to the relative approach flow depth; v is the flow velocity; g is acceleration due to gravity; and d indicates the depth of approach flow. Previous studies (e.g., Kim *et al*. 2017) have highlighted the variation of scour depth per geometric shape of the pile, location, and arrangement. As suggested by Briaud *et al*. (2007) the deterministic approach of scour depth prediction can be converted into a probabilistic one considering the future flood risk. Zhu and Frangopol (2016) and Liao *et al*. (2018) presented probabilistic approaches to risk assessment of bridges under scour. Also, a risk-based cost-benefit analysis for the retrofit of bridges exposed to extreme hydrologic events considering multiple failure modes was presented in Mondoro and

Frangopol (2019). Chow (1965) has suggested the procedure to estimate the discharges of 100-year (Q_{100}) and 500-year (Q_{500}) flood events using linear regression with the help of historical data. The scour depth due to flood risk can be estimated using the framework suggested by Briaud *et al*. (2007), Guo and Chen (2015), and Guo *et al*. (2016). Given known Q_{100} and Q_{500}, the Gaussian parameters (lognormal mean α and standard deviation β) can be estimated by solving Eqs. (24) and (25)

$$P\left(Q > Q_{100}\right) = 1 - \frac{1}{\sigma\sqrt{2\pi}} \int_0^{Q_{100}} \frac{1}{Q} \exp\left(\frac{-\left(\ln Q - \alpha\right)^2}{2\beta^2} \right) dQ \tag{24}$$

$$P\left(Q > Q_{500}\right) = 1 - \frac{1}{\sigma\sqrt{2\pi}} \int_0^{Q_{500}} \frac{1}{Q} \exp\left(\frac{-\left(\ln Q - \alpha\right)^2}{2\beta^2} \right) dQ \tag{25}$$

Subsequently, the expected future stream flow (Q_f) can be computed as (Briaud *et al*. 2011)

$$Q_f = \exp\left(\alpha + x\beta\right) \tag{26}$$

in which x is the standard normal variable. Thereafter, a relationship between discharge and water velocity as well as the relationship between discharge and water depth is obtained using Q_f.

5 **Illustrative Example**

An illustrative example is provided to assess the performance indicators associated with structural vulnerability, long-term resilience and loss. For illustration purpose, it is assumed that the bridge is located at a location exposed to earthquakes and hurricanes over its service life. The selected bridge is a two-span simply supported steel girder bridge with a total length of 40 *m*. The superstructure of bridge has a width of 10.45 *m*, consisting of a deck and six girders. The girder is 1.05 *m* high and the deck is 0.3 *m* thick. A 2D numerical model of bridge is established to evaluate the structural performance under hurricanes. The cross section of the superstructure of this bridge is simplified as shown in Figure 5(a). All the six girders are simplified as rectangles, each of which has a width of 0.3 m and is evenly distributed along the deck. The still water depth is 8m and vertical clearance is set as 4.5 *m*.

5.1 *Vulnerability assessment under natural hazards*

5.1.1 *Structural performance under Hurricanes*

Under the hurricane hazard, the deck unseating failure is considered for this bridge. The wave height and surge elevation are adopted as the *IM*s for the vulnerability analysis. Structural vulnerability is assessed by computing the demand and capacity under hurricanes. The demand of bridge is the total uplift force acting upon the bridge caused by surge and waves, determined by a Finite Element Model (FEM). A 2D model of bridge superstructure under the impact of a hurricane-induced solitary wave is established by CFD software *ANSYS Fluent 17.2 Package* (ANSYS 2016). The numerical diagram of computation domain of the FEM bridge model is illustrated in Figure 5(b).

To verify the numerical results from the ANSYS software, an experimental study at scale 1:30 was conducted at the Hydraulics Laboratory of Hong Kong Polytechnic University, aiming at measuring hurricane loading acting upon the bridge superstructure. This experiment was conducted in an open channel of 27 *m* in length, 1.5 *m* in width, and 1.5 *m* in depth. Waves were generated by a piston-type wavemaker located at one end of the channel. The water elevation was captured by using capacitive wave height gauges. The bridge model was suspended at a certain level according to the surge elevation. The wave forces on the bridge model were measured by a multi-axis load cell. To compare the results to the numerical model, experimental measurements were computed based on the Froude scale model. At the certain surge elevation, the uplift force increases along the growing wave height. Generally, the FEM results were validated by the experiments with acceptable differences. A series of the maximum total uplift forces on bridge superstructure changing over different wave heights were selected to compare them with the numerical results at the surge elevation of 2.2 *m*. The comparison between the FEM results and the experimental results is shown in Figure 6.

The capacity is the vertical resistance of the superstructure, which can be calculated by the sum of static weight and the connection strength between superstructure and substructure. The dead weight of each bridge span is assessed by considering the uncertainties in the density of construction materials and construction and workmanship errors. A normal distribution for concrete and steel density is selected based on data from JCSS (2001). The mean density of reinforced concrete is 2,400 kg/m^3, with a COV of 0.04., while these parameters for steel are 7,850

kg/m^3 and 0.01, respectively. To account for workmanship and construction errors, a uniform PDF for deck thickness is considered with lower and upper limits of 95 and 105% of the as-built plan. The weight of each span per unit length is calculated using Eq. (27) (Ataei and Padgett 2013)

$$W_s = \left(d_b W + A_g \times n_g\right)\gamma \tag{27}$$

where W_s is span weight per unit length; d_b is deck thickness; W is deck width; A_g is the cross-sectional area of the girders; n_g is the number of girders; and γ is unit weight of the material. The connection strength can be determined by comparing the pullout strength and yield strength of the dowel bars. A normal distribution is adopted for concrete strength with a COV of 0.11 (Ellingwood and Hwang 1985).

According to the above structural analyses, the total uplift force and vertical resistance are obtained. Subsequently, the probability of deck unseating is computed by assessing the probability of demand exceeding capacity through MC simulations. Two hurricane scenarios with 100-year (Hurricane scenario one denoted as $\mathbf{H_1}$) and 200-year (Hurricane scenarios two denoted as $\mathbf{H_2}$) return periods are considered. The estimated storm surge for $\mathbf{H_1}$ (100-year) and $\mathbf{H_2}$ (200-year) is 1.74 m and 2.18 m, respectively, according to the surge models of ADCIRC and SLOSH simulations (Lin 2010). The possible storm tide is considered, which is approximately 0.3 to 0.5 m higher than the storm surge level (Lin 2012). Hence, the total surge elevation is evaluated as 2.05 m for $\mathbf{H_1}$ and 2.45 m for $\mathbf{H_2}$, respectively. The wave height for $\mathbf{H_1}$ is 4.60 m and that for $\mathbf{H_2}$ equals 5.35 m using the model demonstrated by Lin (2010). Given these inputs, the probability of deck unseating failure under the investigated two hurricane scenarios $\mathbf{H_1}$ and $\mathbf{H_2}$ are 0.1982 and 0.9013, respectively.

5.1.2 *Structural performance under Earthquakes*

The structural performance of bridge under seismic impacts is assessed. The associated damage caused by earthquakes is independent on that resulted from hurricanes. In this example, the hazard inputs of the selected hazard scenarios are directly provided for the vulnerability analysis. Given more information, the hazard analysis can be conducted using the probabilistic seismic hazard analysis (PSHA) framework, to quantify the uncertainties associated with frequency and seismic magnitude at a given site. The procedures of hazard analysis using the ground motion prediction equation is demonstrated in Appendix B.

Two seismic scenarios with earthquake return period of 75-year (Earthquake scenario one denoted as $\mathbf{E}_1$) and 120-year (Earthquake scenario two denoted as $\mathbf{E}_2$) are considered for the investigated bridge. The associated return period of hazard scenario is the mean of the BPT distribution in the long-term seismic analysis, as shown in Eq. (15). The COV of the BPT distribution is set to 1 (Matthews *et al*. 2002). Given the return periods of earthquake, the PGA values for $\mathbf{E}_1$ and $\mathbf{E}_2$ are determined as 0.1605g and 0.2152g, respectively. The fragility curves can be generated by identifying the seismic demand and capacity selected for the bridge. In this example, a fragility curve for the multi-span simply supported concrete bridges conducted by Nielson and DesRoches (2007) is adopted to assess the system-level vulnerability of bridge. The system fragility is obtained through evaluating the correlated joint probability distribution based on the individual components, consisting of the concrete columns, elastomeric bearing, and abutments in both transverse and longitudinal directions. Using the damage states provided by Nielson and DesRoches (2007), the fragility curves for slight, moderate, major, and complete damage states of the bridge are shown in Figure 7. Thus, the probability of failure of the bridge for scenario $\mathbf{E}_1$ under slight, moderate, major, and complete damage states is 0.3675, 0.0256, 0.0057, and 0.0011, respectively. For scenario $\mathbf{E}_2$, the probability of failure under slight, moderate, major and complete damage states is 0.5449, 0.0670, 0.0189, and 0.0046, respectively.

5.2 *Long-Term Resilience and Loss Quantification*

Given the defined hazard scenarios and fragility inputs, the long-term resilience and loss of the bridge under earthquakes and hurricanes are assessed in this section. The arrivals of earthquakes are modeled by the renewal process with BPT distribution, while a classical Poisson process is used to model the hurricane arrivals. The occurrence rate is taken as the inverse of return period (e.g., the occurrence rate of a 100-year hurricane is 0.01). Two significant inputs for Eqs. (11) and (12) are the resilience and economic repair loss.

In this example, the resilience is assessed by Eq. (2) and the recovery model is based on the model developed by ATC (1999), while any other approaches could also be incorporated during the computational process. By providing recovery actions, the bridge functionality is recovered to a satisfactory level. A similar repair scheme is utilized for bridge under the hurricane induced damage but only the collapse damage is included. The same recovery time from earthquake analysis is utilized for the hurricane damages. The functionality related to the four hazard scenarios

539 is shown in Figure 8. Under the same type of hazard, the bridge under higher level of hazard
540 intensity has a smaller residual functionality, which means the structure requires additional efforts
541 for the recovery. Given the investigated time interval Δt_r = 400 days, the resilience can be
542 calculated using Eq. (2). The bridge resilience under two earthquake hazards $\mathbf{E_1}$ and $\mathbf{E_2}$ is 0.9958
543 and 0.9918, respectively. With the same investigated time interval, the bridge resilience under the
544 hurricane scenarios $\mathbf{H_1}$ and $\mathbf{H_2}$ is computed as 0.9204 and 0.6467, respectively. These four
545 resilience values are considered as the mean resilience inputs for the long-term assessment.
546 Consequently, the expected long-term resilience for earthquakes and hurricanes are computed
547 using Eq. (11), associated with stochastic BPT renewal process and Poisson process, respectively.
548 In a 100-year service life, the expected long-term resilience for the hazard scenarios $\mathbf{E_1}$, $\mathbf{E_2}$, $\mathbf{H_1}$,
549 and $\mathbf{H_2}$ is 1.2835, 0.7536, 0.9204, and 0.3233, respectively. Figure 9 shows the expected long-term
550 resilience under the four scenarios changing over the investigated service life. It is found that the
551 long-term resilience of bridge of scenarios $\mathbf{E_2}$ is the lowest in the first 30 years, while the lowest
552 scenario turns to $\mathbf{H_2}$ in the remaining service life. As a result, decision-makers are required to make
553 appropriate management strategies for the bridge according to the changes of total resilience at
554 different ages.

555 The economic repair loss caused by natural hazard can be computed as the product of
556 rebuilding cost and the probability of failure under the investigated scenario. In this example, the
557 rebuilding cost of bridge is computed as USD 963,908, based on the consequence evaluation
558 parameters provided by Zheng *et al.* (2018). For bridge damaged by deck unseating during
559 hurricanes, the rebuilding cost is mainly due to the repair of superstructure, taken as 40% of the
560 rebuilding cost (Mondoro *et al*. 2017). The expectation of long-term loss of the bridge under
561 earthquake and hurricane is computed using Eq. (12), including inputs of the occurrence rate of
562 investigated hazard, service life, hazard intensity, and financial discount rate. The economic repair
563 loss for the hazard scenarios $\mathbf{E_1}$, $\mathbf{E_2}$, $\mathbf{H_1}$, and $\mathbf{H_2}$ is USD 0.1909×10^5, 0.4019×10^5, 7.6419×10^5,
564 and 3.4751×10^5, respectively. The service life remains 100 years and a financial discount rate of
565 3% is used. Based on the renewal model, the expected long-term damage loss under the hazard
566 scenarios $\mathbf{E_1}$, $\mathbf{E_2}$, $\mathbf{H_1}$, and $\mathbf{H_2}$ is USD 0.629×10^4, 0.679×10^4, 2.420×10^4, and 5.503×10^4,
567 respectively. Figure 10(a) shows the expected long-term damage loss changing over investigated
568 period under the four scenarios.

It is identified from the long-term damage loss that the bridge is exposed to dominated hurricane hazard scenario $\mathbf{H_2}$, which leads to the highest expected long-term loss throughout the investigated period. This outcome is reasonable since the bridge has the largest probability of failure and a relatively high repair cost under the hazard scenario $\mathbf{H_2}$. On the contrary, the hazard scenario $\mathbf{E_1}$ and $\mathbf{E_2}$ can cause the lowest long-term loss of the bridge. Due to the stochastic time-independent HPP model, the expected long-term damage loss of hurricane scenario $\mathbf{H_2}$ is consistently higher than that of scenario $\mathbf{H_1}$, as shown in Figure 10(a). However, the changing pattern of long-term damage loss under two earthquake scenarios is different, as shown in Figure 10(b), due to the time-varying occurrence rate in the BPT renewal process. When the service life is smaller than 55 years, the total damage loss of scenario $\mathbf{E_1}$ is larger than $\mathbf{E_2}$ but the situation is opposite in the remaining 45 years. Therefore, the decision-makers should consider both the long-term resilience and damage loss, as only focusing on the long-term loss may lead to inappropriate decisions. For instance, though the long-term loss of scenario $\mathbf{H_2}$ is the highest throughout the investigated period, the long-term resilience of $\mathbf{E_2}$ is the lowest when the bridge service life is smaller than 30 years.

The above results obtained through the analytical renewal-based approach is validated by the MC simulations. The stochastic renewal process is constructed by modelling the interarrival times according to the given probability distribution. The interarrival times having BPT distribution are modeled using the inverse transform sampling. Consequently, the expected long-term loss and resilience are computed using the Eqs. (5) and (6). Through the MC approach, the expected long-term resilience for the hazard scenarios $\mathbf{E_1}$, $\mathbf{E_2}$, $\mathbf{H_1}$, and $\mathbf{H_2}$ is 1.2819, 0.7531, 0.9208, and 0.3233, respectively, for a 100-year service life. The associated expected long-term damage loss under the hazard scenarios $\mathbf{E_1}$, $\mathbf{E_2}$, $\mathbf{H_1}$, and $\mathbf{H_2}$ is USD 0.637×10^4, 0.699×10^4, 2.461×10^4, and 5.595×10^4, respectively. Overall, these numerical results have an acceptable agreement on the analytical outcomes.

For the dominant scenario $\mathbf{H_2}$, the expected long-term loss is sensitive to the change of financial discount rate and the economic repair loss as shown in Figure 11(a) and 11(b), respectively. The long-term loss with a discount rate at 1% is nearly three times larger than that with a discount rate at 4%. Therefore, identifying the appropriate value for discount rate is essential for the long-term loss evaluation. In addition, the long-term loss can be significantly enlarged by the increase of economic repair loss. By defining the original economic repair loss for scenario $\mathbf{H_2}$

as L_0, the expectation of long-term loss affected by triple, double, a half and a third of L_0 is shown in Figure 11(b). Since the economic repair loss highly depends on the vulnerability analysis in terms of the probability of failure, it indicates the large uncertainty related to fragility curves during the long-term loss estimation. Based on the outcomes, decision-makers can further decide the risk mitigation strategies associated with this dominated scenario.

6 **Conclusions**

This paper provides an elaborate framework for the long-term resilience and long-term loss assessment of highway bridges under multiple hazards. The independent natural hazards are focused. The common approach of resilience assessment, the resilience quantification based on practical engineering considerations, and the long-term resilience and loss estimation according to the stochastic renewal process are introduced. Time-independent and time-varying hazard occurrence characteristics are incorporated in the analysis using the stochastic renewal process. Uncertainties arising from the occurrence of extreme events, structural vulnerability and the resulting consequences caused by the hazards are considered. Several typical natural hazards (i.e. earthquakes, hurricanes and floods) are outlined and the corresponding performance scenarios are discussed. The proposed approach is illustrated on a typical highway bridge. A numerical model is constructed to assess the structural performance of bridge under hurricane hazard, which is validated by the experimental tests. The time-dependent functionalities under recovery patterns for four different hazard scenarios are calculated. The bridge resilience under each hazard scenario is evaluated.

In addition, the presented approach allows successful estimation of the long-term resilience and loss by identifying the major distribution characteristics of damage cost of existing bridges. A stochastic renewal process is applied to derive the expectation of long-term resilience and damage loss. Different stochastic models are applied to model the hazard occurrence, in which the BPT renewal process and Poisson process are adopted for earthquake and hurricane, respectively. The long-term resilience and loss are quantified for the four selected hazard scenarios.

The results reveal that the hurricane with a 200-year return period is the costliest hazard for the bridge. Though the long-term loss caused by the 200-year hurricane is the highest throughout

the investigated 100-year service life, the long-term resilience of the earthquake with a 120-year return period is the lowest in the first 30 years. Thus, decision-makers are expected to consider both the long-term resilience and damage loss. The long-term loss significantly depends on occurrence and intensity of the hazard, remaining service life and financial discount rate. Careful evaluations on the financial discount rate and the structural fragility analysis are important. Based on the results presented, decision makers can decide the risk mitigation strategies associated with various hazard scenarios. The approach presented can benefit insurers and policy-makers to manage bridges against the impacts of multiple hazards in a life-cycle context. Further studies are expected to consider the interdependencies and interactions of hazardous events. The life-cycle management can be further incorporated into the proposed framework by considering the intervention actions (e.g., inspection, maintenance, and repair) to deliver the optimal solution for decision-makers.

Acknowledgements

The study has been supported by The Hong Kong Polytechnic University under Start-Up Fund 1-ZE7Q, the National Natural Science Foundation of China (Grant No. 51808476), the Research Grant Council of Hong Kong (ECS project No. PolyU 252161/18E), and the U.S. National Science Foundation through grant CMMI-1537926. The support is gratefully acknowledged. The authors gratefully acknowledge Mr. Deming Zhu for the sketch of CFD model and Mr. Jing Qian for the support in terms of resilience computation. The opinions and conclusions presented in this paper are those of the authors and do not necessarily reflect the views of the sponsoring organizations.

Appendix A. Expected long-term resilience and loss

The derivation of long-term resilience and loss in Eqs. (11) and (12) are provided. The expected long-term resilience can be determined by the properties of compound stochastic process (Ross 2014), which equals the sum of number of arrivals times the expected resilience

$$E[RE_{lt}(t_{\max})] = E[R_k]E[N(t_{\max})] = E[R_k]\Phi(t_{\max}) \tag{A1}$$

For the discounted long-term loss, the expectation can be written into two parts by conditioning on the first renewal time y

$$\begin{aligned} E[DL_{lt}(t_{\max})] &= E\left[E[e^{-ry}L_1 + e^{-ry}DL_{lt}(t_{\max}-y)\middle| W_1 = y] \right] \\ &= E[L]\int_0^{t_{\max}} e^{-ry}dF_W(y) + E[L]\int_0^{t_{\max}} e^{-ry}E\left[\sum_{k=1}^{(t_{\max}-y)} e^{-rT_k}\right]dF_W(y) \end{aligned} \tag{A2}$$

in which the CDF of interarrival time F_W in a finite time domain is a defective distribution for interarrival time, denoted as $\psi(t_{\max})$ (Léveillé and Garrido 2001; Rolski *et al*. 2009). In an infinite time horizon, the defective distribution is the Laplace transform of F_W, denoted as $\psi_r(\infty)$.

$$\psi(t_{\max}) = \int_0^{t_{\max}} e^{-rs} f_W(s)ds = \int_0^{t_{\max}} e^{-rs}dF_W(s) \tag{A3}$$

Using this notation, the expected long-term loss is expressed as

$$E\left[DL_{lt}(t_{\max})\right] = E[L]\psi(t_{\max}) + E[L]E\left[\sum_{k=1}^{N(\cdot)} e^{-rT_k}\right] * \psi(t_{\text{int}}) = E[L]\sum_{k=1}^{\infty}\psi^{(k)}(t_{\text{int}}) \tag{A4}$$

To connect Eq. (A4) with the expected number of arrivals of hazards in the renewal process, the convolution power of $\psi(t_{\max})$ is computed

$$\begin{aligned} \psi^{(k+1)}(t_{\max}) &= \int_0^{t_{\max}} e^{-rs}\psi^{(k)}(t_{\max}-s)dF_W(s) = \int_0^{t_{\max}}\int_0^{t_{\max}-s} e^{-r(s+v)}dF_W{}^{(k)}(v)dF_W(s) \\ &= \int_0^{\infty} e^{-rs}I_{\{0,t_{\max}\}}(s)dF_W{}^{(k+1)}(s) = \int_0^{t_{\max}} e^{-rs}dF_W{}^{(k+1)}(s) \end{aligned} \tag{A5}$$

where $I_A(\cdot)$ represents the indicator function of a set A. It equals to one only if A is true but equals to zero otherwise: e.g., $I_{\{0,\,t\max\}}(s)$ equals to one if $0 \le s \le t_{\max}$. Since the renewal function is the k-fold convolution of the PDF of interarrival time, the Eq. (A5) is rearranged as follows

$$\sum_{k=1}^{\infty}\psi^{(k)}(t_{\max}) = \int_0^{t_{\max}} e^{-rs}d\sum_{k=1}^{\infty}F_W{}^{(k)}(s) = \int_0^{t_{\max}} e^{-rs}d\Phi(s) \tag{A6}$$

Substituting Eq. (A6) into the Eq. (A4), the expected long-term loss is

$$E[DL_{lt}(t_{\max})] = E[L]\int_0^{t_{\max}} e^{-rs} d\Phi(s) \quad \text{(A7)}$$

Appendix B. Probabilistic seismic hazard analysis

The probabilistic seismic hazard analysis framework quantifies various uncertainties from location, size and intensity of an earthquake, among others to present an explicit distribution of future ground motions. The process of computing the rate of earthquake occurrence is presented.

Gutenberg and Richter (1944) provided the recurrence relationship between earthquake frequency and magnitude based on

$$\log_{10} \lambda_m = a - bm \quad \text{(B1)}$$

where λ_m is the rate of earthquakes with magnitudes greater than m; and a and b are coefficients.

Considering the minimum and maximum magnitudes associated with a finite fault, a bounded CDF for the magnitudes of earthquakes can be derived as

$$F_M(m) = \frac{1-10^{-b(m-m_{\min})}}{1-10^{-b(m_{\max}-m_{\min})}},\ m_{\min} < m < m_{\max} \quad \text{(B2)}$$

where $F_M(m)$ is the CDF for magnitude; $m_{\max}$ is the maximum magnitude that a given source can produce; and $m_{\min}$ is the minimum magnitude considered in the analysis.

Depending on the characteristics of earthquakes, the ground motion prediction models (GMPM) can predict the expected levels of ground motion intensity. Boore *et al*. (2014) provided a ground motion prediction model, given by

$$\ln IM = F_E(M, mech) + F_P(R_{JB}, M, region) + F_S(V_{S30}, R_{JB}, M, z_1) + \varepsilon_n \sigma(M, R_{JB}, V_{S30}) \quad \text{(B3)}$$

where lnIM is the natural logarithm of a ground motion intensity measure; F_E, F_P, and F_S are functions for source, path, and site parameters, respectively; ε_n is the fractional number of standard deviations of a single predicted value of lnIM away from the mean; and σ is the total standard deviation of the model.

682 The total standard deviation is given by

$$\sigma(M, R_{JB}, V_{S30}) = \sqrt{\phi^2(M, R_{JB}, V_{S30}) + \tau^2(M)} \quad \text{(B4)}$$

683 where τ is the M-dependent between-event standard deviation; and ϕ is the M-, R_{JB}- and V_{S30}-
684 dependent within-event standard deviation.

685 With the mean and standard deviation from this GMPM model, the exceedance probability of
686 a *PGA* level can be computed under the given magnitude and site conditions

$$P(IM > x \mid m, r) = 1 - \Phi\left(\frac{\ln x - \overline{\ln IM}}{\sigma_{\ln IM}}\right) \quad \text{(B5)}$$

687 where Φ (.) is the standard normal CDF; $\overline{\ln IM}$ is the mean of lnIM; and $\sigma_{\ln IM}$ is the standard
688 deviation of lnIM. The normal distribution parameters are output from the GMPM.

689 Consequently, the annual rate of exceeding a given intensity measure can be derived using the
690 total probability theorem

$$\lambda(IM > x) = \sum_{i=1}^{n_{source}} \lambda(M_i > m_{\min}) \int_{m_{\min}}^{m_{\max}} \int_{0}^{r_{\max}} P(IM > x \mid m, r) f_{Mi}(m) f_{Ri}(r) dr dm \quad \text{(B6)}$$

691 where $\lambda(M_i > m_{\min})$ is the rate of occurrence of earthquakes greater than $m_{\min}$ from source i; $\lambda(IM >$
692 $x)$ is the annual rate of intensity measure greater than x; n_{source} is the number of sources considered;
693 $f_{Mi}(m)$ is the PDF for magnitude from source i; and $f_{Ri}(r)$ is the PDF of distance for source i. The
694 inverse of the annual probability of exceedance is known as the return period. The seismic intensity
695 measure values for different return periods can be determined accordingly.

696 **References**

697 AASHTO (2000). *AASHTO LRFD Bridge Design Specifications*. Washington, DC.

698 AASHTO (2008). *AASHTO guide specifications for bridges vulnerable to coastal storms*.
699 Washington, DC.

Akiyama, M., Frangopol, D.M., and Ishibashi, H. (2019). Toward life-cycle reliability-, risk-, and resilience-based design and assessment of bridges and bridge networks under independent and interacting hazards: Emphasis on earthquake, tsunami and corrosion. *Structure and Infrastructure Engineering*. doi: 10.1080/15732479.2019.1604770

Akiyama, M., Frangopol, D. M., and Matsuzaki, H. (2011). Life-cycle reliability of RC bridge piers under seismic and airborne chloride hazards. *Earthquake Engineering and Structural Dynamics*, 40(15), 1671-1687.

ANSYS (2016). *ANSYS Fluent Theory Guide, Release 17.2*. ANSYS Inc. Southpointe, Canonsburg.

Ataei, N., and Padgett, J. E. (2013). Probabilistic modeling of bridge deck unseating during hurricane events. *Journal of Bridge Engineering*, 18(4), 275-286.

ATC (1999). Earthquake damage evaluation data for California. *Technical Report ATC-13*, Applied Technology Council, Redwood City, CA.

Bocchini, P., and Frangopol, D.M. (2011). A probabilistic computational framework for bridge network optimal maintenance scheduling. *Reliability Engineering and System Safety*, 96(2), 332-349.

Bocchini, P., and Frangopol, D. M. (2012). Restoration of bridge networks after an earthquake: Multicriteria intervention optimization. *Earthquake Spectra*, 28(2), 426-455.

Boore, D. M., Stewart, J. P., Seyhan, E., and Atkinson, G. M. (2014). NGA-West2 equations for predicting PGA, PGV, and 5% damped PSA for shallow crustal earthquakes. *Earthquake Spectra*, 30(3), 1057-1085.

Briaud, J. L., Brandimarte, L., Wang, J., and D'odorico, P. (2007). Probability of scour depth exceedance owing to hydrologic uncertainty. *Georisk*, 1(2), 77-88.

Broccardo, M., Galanis, P., Esposito, S., and Stojadinovic, B. (2015). Probabilistic resilience assessment of civil systems: Analysis and validity of the PEER framework. *Safety and Reliability of Complex Engineered Systems: ESREL* 2015, 331.

Bruneau, M., Barbato, M., Padgett, J. E., Zaghi, A. E., Mitrani-Reiser, J., and Li, Y. (2017). State of the Art of Multihazard Design. *Journal of Structural Engineering*, 143(10), 03117002.

Bruneau, M., Chang, S.E., Eguchi, R.T., Lee, G.C., O'Rourke, T.D., Reinhorn, A.M., Shinozuka, M., Tierney, K., Wallace, W.A., and Winterfeldt, D.V. (2003). A framework to quantitatively assess and enhance the seismic resilience of communities. *Earthquake Spectra*, 19(4), 733–752.

Chow, V. T. (1965). Bibliography: 1) Handbook of Applied Hydrology. International Association of Scientific Hydrology. Bulletin, 10(1), 82-83.

Cimellaro, G.P., Reinhorn, A.M., and Bruneau, M. (2010). Seismic resilience of a hospital system. *Structure and Infrastructure Engineering*, 6(1-2), 127–144.

Cornell, A.C., Jalayer, F., and Hamburger R.O. (2002). Probabilistic basis for 2000 SAC federal emergency management agency steel moment frame guidelines. *Journal of Structural Engineering*, 128(4), 526–532.

Decò, A., Bocchini, P., and Frangopol, D. M. (2013). A probabilistic approach for the prediction of seismic resilience of bridges. *Earthquake Engineering and Structural Dynamics*, 42(10), 1469-1487.

Decò, A., and Frangopol, D. M. (2011). Risk assessment of highway bridges under multiple hazards. *Journal of Risk Research*, 14(9), 1057-1089.

Decò, A., Frangopol, D.M., and Bocchini, P. (2013). Probabilistic seismic resilience of bridge networks. *The 11th International Conference on Safety, Reliability, Risk and Life-Cycle Performance of Structures and Infrastructures*, 621-628.

Dong, Y., and Frangopol, D.M. (2015). Risk and resilience assessment of bridges under mainshock and aftershocks incorporating uncertainties. *Engineering Structures*, 83, 198-208.

Dong, Y., and Frangopol, D.M. (2016). Time-dependent multi-hazard life-cycle assessment of bridges considering climate change. *Journal of Performance of Constructed Facilities*, 30(5), 04016034, 1-12.

752 Dong, Y., and Frangopol, D.M. (2017). Probabilistic life-cycle cost-benefit analysis of portfolios
753 of buildings under flood hazard. *Engineering Structures*, 142, 290-299.

754 Ellingwood, B., and Hwang, H. (1985). Probabilistic descriptions of resistance of safety-related
755 structures in nuclear plants. *Nuclear Engineering and Design*, 88(2), 169-178.

756 Franchin, P., and Cavalieri, F. (2015). Probabilistic assessment of civil infrastructure resilience to
757 earthquakes. *Computer-Aided Civil and Infrastructure Engineering*, 30(7), 583-600.

758 Frangopol, D. M. (2011). Life-cycle performance, management, and optimization of structural
759 systems under uncertainty: Accomplishments and Challenges. *Structure and Infrastructure*
760 *Engineering*, 7(6), 389-413.

761 Frangopol, D. M., and Soliman, M. (2016). Life-cycle of structural systems: recent achievements
762 and future directions. *Structure and Infrastructure Engineering*, 12(1), 1-20.

763 Frangopol, D.M., Dong, Y., and Sabatino, S. (2017). Bridge life-cycle performance and cost:
764 Analysis, prediction, optimization and decision making. *Structure and Infrastructure*
765 *Engineering*, 13(10), 1239-1257.

766 Gautam, D. (2017). On seismic vulnerability of highway bridges in Nepal: 1988 Udaypur
767 earthquake (MW 6.8) revisited. *Soil Dynamics and Earthquake Engineering*, 99, 168-171.

768 Gautam, D., and Dong, Y. (2018). Multi-hazard vulnerability of structures and lifelines due to the
769 2015 Gorkha earthquake and 2017 central Nepal flash flood. *Journal of Building*
770 *Engineering*, 17, 196-201.

771 Gidaris, I., Padgett, J. E., Barbosa, A. R., Chen, S., Cox, D., Webb, B., and Cerato, A. (2017).
772 Multiple-hazard fragility and restoration models of highway bridges for regional risk and
773 resilience assessment in the United States: state-of-the-art review. *Journal of structural*
774 *engineering*, 143(3), 04016188.

775 Guo, X., and Chen, Z. (2015). Lifecycle multihazard framework for assessing flood scour and
776 earthquake effects on bridge failure. *ASCE-ASME Journal of Risk and Uncertainty in*
777 *Engineering Systems, Part A: Civil Engineering*, 2(2), C4015004.

778 Guo, X., Wu, Y., and Guo, Y. (2016). Time-dependent seismic fragility analysis of bridge systems
779 under scour hazard and earthquake loads. *Engineering Structures*, 121, 52-60.

780 Gutenberg, B., and Richter, C. F. (1944). Frequency of earthquakes in California. *Bulletin of the*
781 *Seismological society of America*, 34(4), 185-188.

782 Hainzl, S., Scherbaum, F., and Beauval, C. (2006). Estimating background activity based on
783 interevent-time distribution. *Bulletin of the Seismological Society of America*, 96(1), 313-
784 320.

785 Hashemi, M. J., Al-Attraqchi, A. Y., Kalfat, R., and Al-Mahaidi, R. (2019). Linking seismic
786 resilience into sustainability assessment of limited-ductility RC buildings. *Engineering*
787 *Structures*, 188, 121-136.

788 FEMA (2013). HAZUS Tsunami methodology technical manual. Federal Emergency
789 Management Agency (FEMA). Washington, DC.

790 ISO (2009). Risk management – Principles and guidelines. *International Organization for*
791 *Standardization*, Geneva, Switzerland.

792 Jalayer, F., Asprone, D., Prota, A., and Manfredi, G. (2011). Multi-hazard upgrade decision
793 making for critical infrastructure based on life-cycle cost criteria. *Earthquake Engineering*
794 *and Structural Dynamic*, 40, 1163-1179.

795 JCSS (2001). JCSS Probabilistic model code. 3: Resistance models. *Joint Committee on*
796 *Structural Safety*.

797 Kameshwar, S., and Padgett, J. E. (2014). Multi-hazard risk assessment of highway bridges
798 subjected to earthquake and hurricane hazards. *Engineering Structures*, 78, 154-166.

799 Kilanitis, I., and Sextos, A. (2019). Integrated seismic risk and resilience assessment of roadway
800 networks in earthquake prone areas. *Bulletin of earthquake engineering*, 17(1), 181-210.

801 Kim, H., Sim, S. H., Lee, J., Lee, Y. J., and Kim, J. M. (2017). Flood fragility analysis for bridges
802 with multiple failure modes. *Advances in Mechanical Engineering*, 9(3),
803 1687814017696415.

804 Kohnke, P. (1994). *ANSYS Theory Reference Manual*. ANSYS Inc., Canonsburg, USA.

Léveillé, G., and Garrido, J. (2001). Recursive moments of compound renewal sums with discounted claims. *Scandinavian Actuarial Journal*, *2001*(2), 98-110.

Liao, K. W., Muto, Y., and Gitomarsono, J. (2018). Reliability analysis of river bridge against scours and earthquakes. *Journal of Performance of Constructed Facilities*, 32(3), 04018017.

Lin, N., Emanuel, K. A., Smith, J. A., and Vanmarcke, E. (2010). Risk assessment of hurricane storm surge for New York City. *Journal of Geophysical Research: Atmospheres*, 115(D18).

Lin, N., Emanuel, K., Oppenheimer, M., and Vanmarcke, E. (2012). Physically based assessment of hurricane surge threat under climate change. *Nature Climate Change*, 2(6), 462.

Matthews, M. V., Ellsworth, W. L., and Reasenberg, P. A. (2002). A Brownian model for recurrent earthquakes. *Bulletin of the Seismological Society of America*, 92(6), 2233-2250.

Michael, A. J. (2005). Viscoelasticity, postseismic slip, fault interactions, and the recurrence of large earthquakes. *Bulletin of the Seismological Society of America*, 95(5), 1594-1603.

Minaie, E., and Moon, F. (2017). Practical and simplified approach for quantifying bridge resilience. *Journal of Infrastructure Systems*, 23(4), 04017016.

Moehle, J., and Deierlein, G. (2004). A framework methodology for performance-based earthquake engineering. *The 13th World Conference on Earthquake Engineering*, 679.

Mondoro, A., and Frangopol, D.M. (2019). Risk-based cost-benefit analysis for the retrofit of bridges exposed to extreme hydrologic events considering multiple failure modes. *Engineering Structures*, 159, 310-319.

Mondoro, A., Frangopol, D.M., and Soliman, M. (2017). Optimal risk-based management of coastal bridges vulnerable to hurricanes. *Journal of Infrastructure Systems*, 23 (3), 2017, 04016046.

Nielson, B. G., and DesRoches, R. (2007). Analytical seismic fragility curves for typical bridges in the central and southeastern United States. *Earthquake Spectra*, 23(3), 615-633.

Padgett, J.E., DesRoches, R., Nielson, B., Yashinsky, M., Kwon, O.S., Burdette, N. and Tavera, E. (2008). Bridge damage and repair costs from Hurricane Katrina. *Journal of Bridge Engineering*, 13(1), 6-14.

Padgett, J.E., Ghosh, J., and Dennemann, K. (2009). Sustainable infrastructure subjected to multiple threats. *TCLEE 2009: Lifeline Earthquake Engineering in a Multi-Hazard Environment*, 703-713.

Pandey, M. D., and Van Der Weide, J. A. M. (2017). Stochastic renewal process models for estimation of damage cost over the life-cycle of a structure. *Structural Safety*, 67, 27-38.

PEER (Pacific Earthquake Engineering Research Center) (2013). *PEER Ground Motion Database*, University of California, Berkeley, CA.

Pescaroli, G., Wicks, R. T., Giacomello, G., and Alexander, D. E. (2018). Increasing resilience to cascading events: The M. OR. D. OR. scenario. *Safety Science*, 110, 131-140.

Qeshta, I. M., Hashemi, M. J., Gravina, R., and Setunge, S. (2019). Review of resilience assessment of coastal bridges to extreme wave-induced loads. *Engineering Structures*, 185, 332-352.

Rolski, T., Schmidli, H., Schmidt, V., and Teugels, J. L. (2009). *Stochastic processes for insurance and finance* (Vol. 505). John Wiley and Sons.

Ross, S. M. (2014). *Introduction to probability models*. Amsterdam: Academic Press.

Thanapol, Y., Akiyama, M., and Frangopol, D. M. (2016). Updating the seismic reliability of existing RC structures in a marine environment by incorporating the spatial steel corrosion distribution: Application to bridge piers. *Journal of Bridge Engineering*, 21(7), 04016031.

Thoft-Christensen, P., Jensen, F. M., Middleton, C. R., and Blackmore, A. (1997). Revised rules for concrete bridges. *Safety of Bridges*, 175-188.

Wang, C., Zhang, H., Feng, K., and Li, Q. (2017). Assessing hurricane damage costs in the presence of vulnerability model uncertainty. *Natural Hazards*, 85(3), 1621-1635.

Wang, Z., Padgett, J. E., and Dueñas-Osorio, L. (2014). Risk-consistent calibration of load factors for the design of reinforced concrete bridges under the combined effects of earthquake and scour hazards. *Engineering Structures*, 79, 86-95.

Yang, D. Y., and Frangopol, D.M. (2018). Risk-informed bridge rating at project and network levels. *Journal of Infrastructure Systems*, ASCE, 24(3), 04018018, 1-13.

Yang, D.Y., and Frangopol, D.M. (2019a). Life-cycle management of deteriorating civil infrastructure considering resilience to lifetime hazards: A general approach based on renewal-reward processes. *Reliability Engineering and System Safety*, 183, 197-212.

Yang, D.Y., and Frangopol, D.M. (2019b). Societal risk assessment of transportation networks under uncertainties due to climate change and population growth. *Structural Safety*, 78, 33-47.

Yanmaz, A. M. (2001). Uncertainty of local scouring parameters around bridge piers. *Turkish Journal of Engineering and Environmental Sciences*, 25(2), 127-137.

Zhang, N., Alipour, A., and Coronel, L. (2018). Application of novel recovery techniques to enhance the resilience of transportation networks. Transportation research record, 2672(1), 138-147.

Zhang, Q., and Alam, M. S. (2019). Performance-based seismic design of bridges: a global perspective and critical review of past, present and future directions. *Structure and Infrastructure Engineering*, 15(4), 539-554.

Zhang, W., Wang, N., and Nicholson, C. (2017). Resilience-based post-disaster recovery strategies for road-bridge networks. Structure and Infrastructure Engineering, 13(11), 1404-1413.

Zheng, Y., and Dong, Y. (2019). Performance-based assessment of bridges with steel - SMA reinforced piers in a life-cycle context by numerical approach. *Bulletin of Earthquake Engineering*, 17(3), 1667-1688.

Zheng, Y., Dong, Y., and Li, Y. (2018). Resilience and life-cycle performance of smart bridges with shape memory alloy (SMA)-cable-based bearings. *Construction and Building Materials*, 158, 389-400.

882 Zhu, B., and Frangopol, D.M. (2016). Time-variant risk assessment of bridges with partially and
883 fully closed lanes due to traffic loading and scour. *Journal of Bridge Engineering*, 21(6),
884 04016021.

885

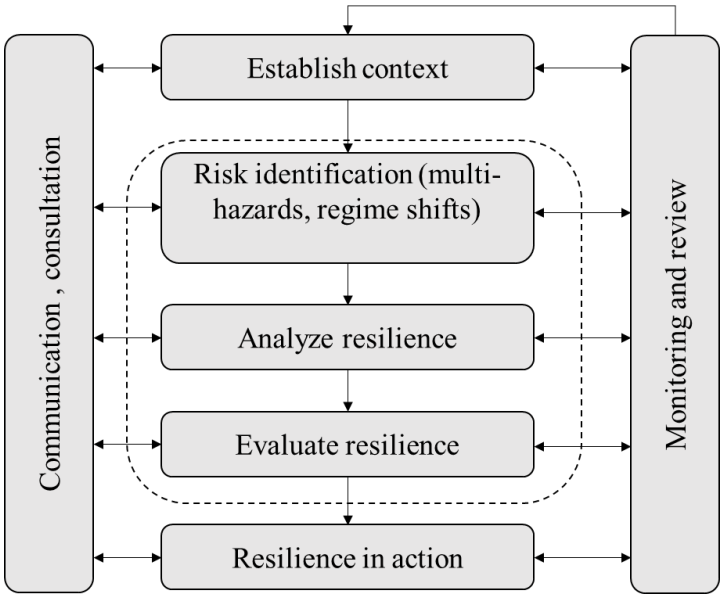

Figure 1. Resilience assessment framework (adapted from ISO 2009).

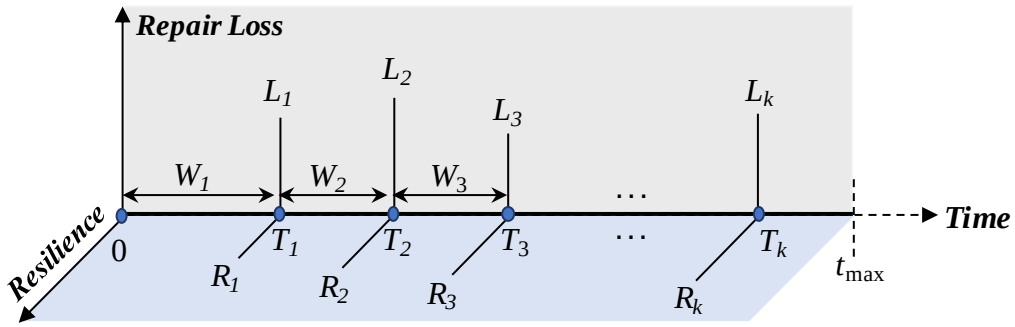

Figure 2. The long-term resilience and loss framework based on stochastic renewal process.

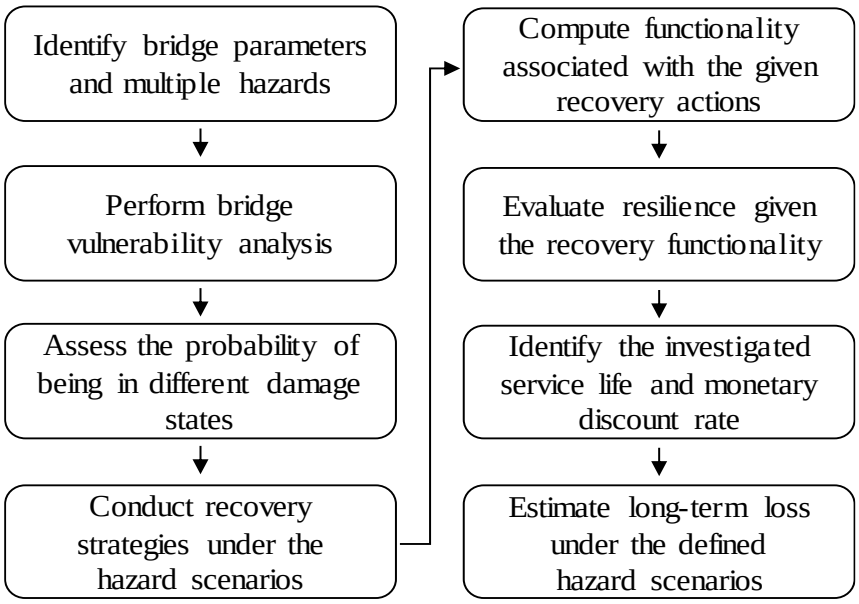

Figure 3. Computational framework integrating resilience and loss assessment.

(a) (b)

Figure 4. (a) Collapsed and washed away bridge due to 2017 flood in Nepal and (b) scouring observed in a bridge in Nepal after the 2017 central Nepal flash flood (two photos taken by the fourth author).

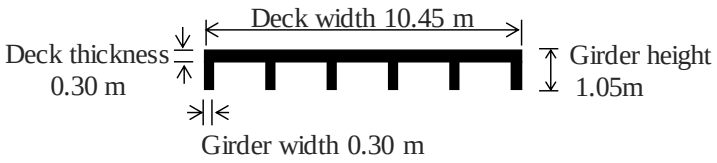

(a)

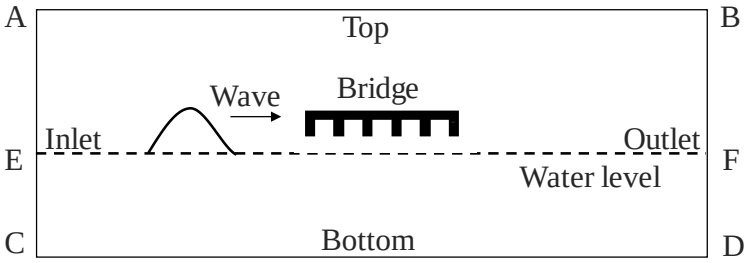

(b)

Figure 5. (a) Geometry of bridge superstructure and (b) numerical diagram of computation domain of the FEM model.

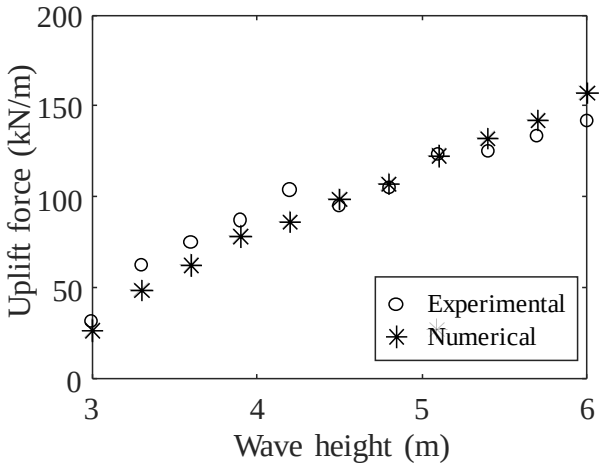

Figure 6. Comparison between numerical and experimental results of the maximum total uplift force acting on the bridge superstructure.

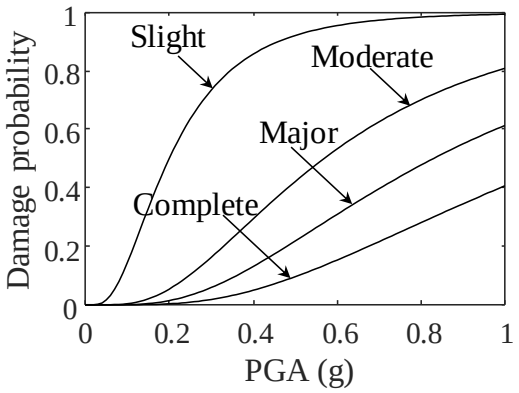

914

915 Figure 7. System-level fragility curves for the bridge at different damage stages (adapted from
916 Nielson and DesRoches 2007).

917

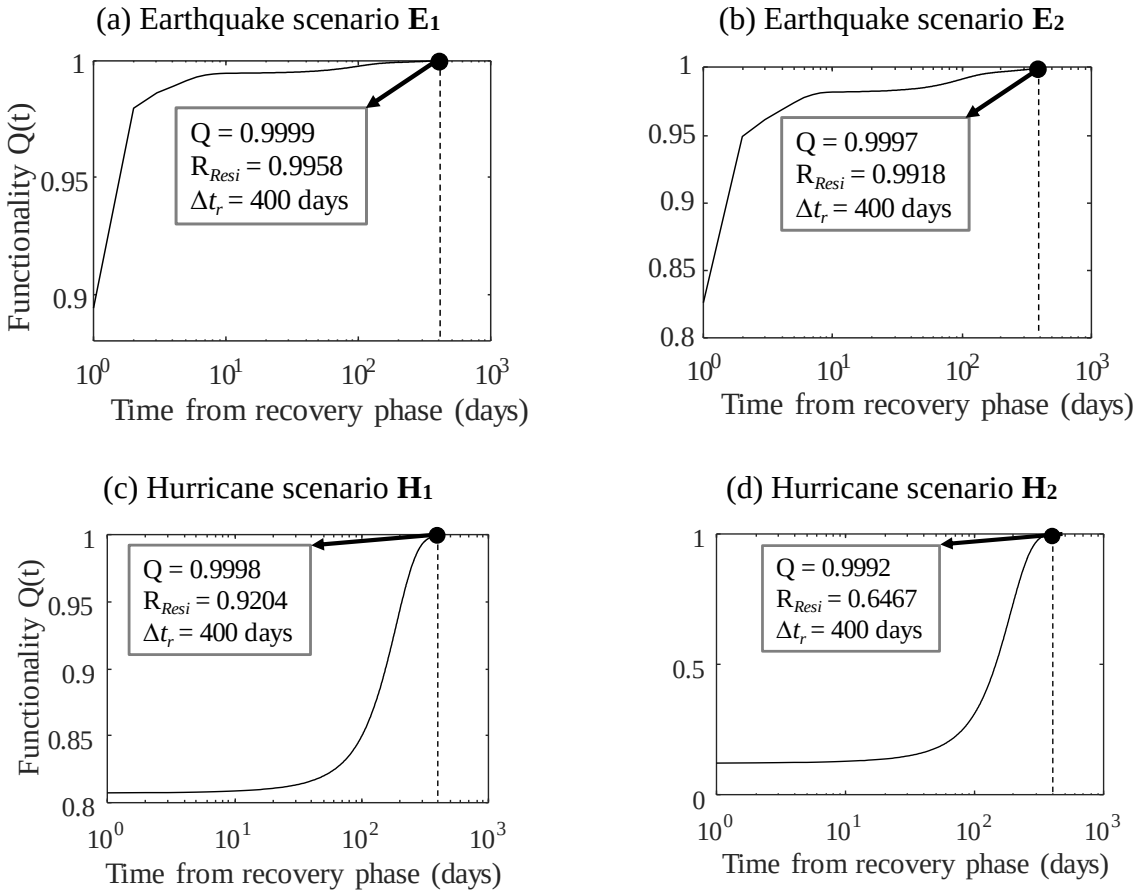

918 Figure 8. Time-dependent functionality of four investigated hazard scenarios (**E1**, **E2**, **H1**, and
919 **H2**).

920

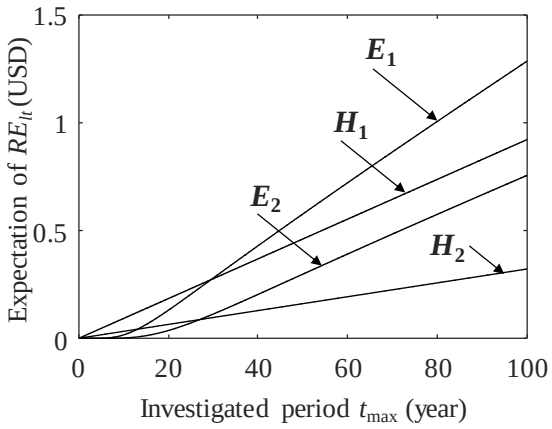

Figure 9. Long-term resilience for the investigated bridge under earthquake and hurricane hazards using renewal method.

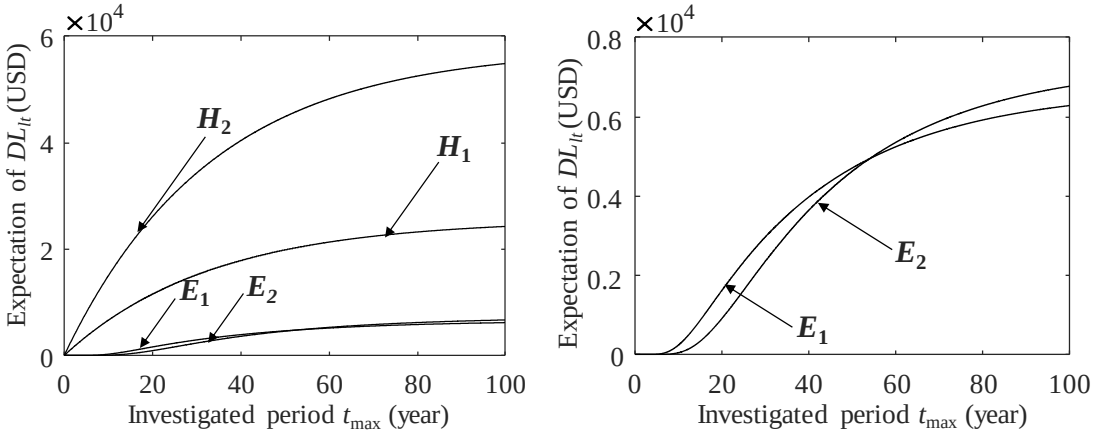

(a) (b)

Figure 10. Long-term damage loss estimation for the investigated bridge under earthquake and hurricane hazards using renewal method (a) for four hazard scenarios (b) for seismic scenario **E**$_1$ and **E**$_2$.

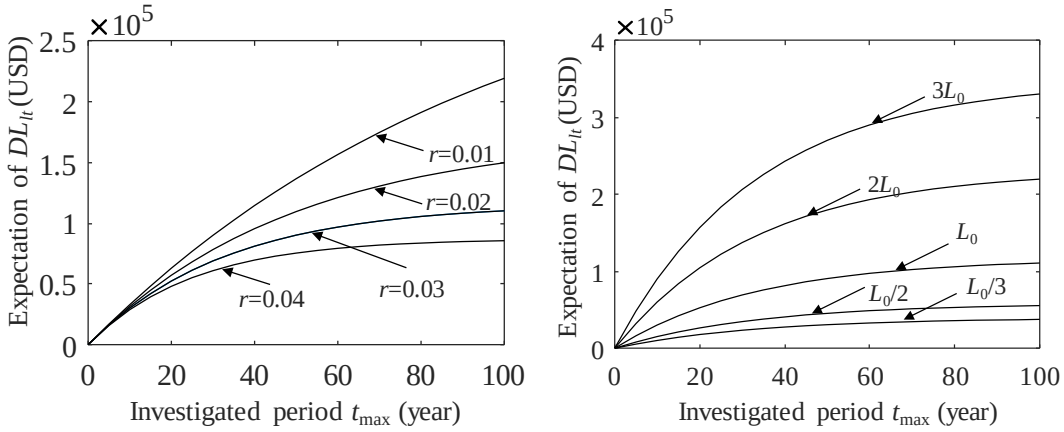

(a) (b)

Figure 11. Expected long-term damage loss affected by (a) financial discount ratio and (b) economic repair loss.